Elias Pentti, Juho Rysti, Anssi Salmela, Alexander Sebedash, and Juha Tuoriniemi. 2009. Studies on helium liquids by vibrating wires and quartz tuning forks. Espoo, Finland. 36 pages. Helsinki University of Technology, Low Temperature Laboratory Publications, Report TKK-KYL-021.

Studies on Helium Liquids by Vibrating Wires and Quartz Tuning Forks

Elias Pentti, Juho Rysti, Anssi Salmela,
Alexander Sebedash, and Juha Tuoriniemi

Low Temperature Laboratory, Helsinki University of Technology,
P.O. Box 5100, FI-02015 TKK, Finland

REPORT TKK-KYL-020

April 2009

ISBN 978-951-22-9863-1
ISSN 1455-0806

Abstract

We present results of low-temperature experiments on dilute mixtures of ^{3}He in ^{4}He and on pure ^{3}He, obtained by means of two kinds of mechanical oscillators immersed in the liquid sample: vibrating wires and quartz tuning forks. The measured effect of the surrounding fluid on the mechanical resonance of the oscillators is compared with existing theories. We also discuss resonances of second sound and the state of supersaturation, both observed by a tuning fork in helium mixtures.

Contents

1 Introduction

Dilute mixture of ^{3}He in ^{4}He is a fascinating subject of research as the only liquid solution that remains miscible down to the absolute zero. Although the two helium isotopes are chemically identical, their fundamental difference manifests itself at millikelvin temperatures: the bosonic ^{4}He component is practically in its ground state, a perfect superfluid, whereas the ^{3}He component forms a unique example of an uncharged, weakly interacting degenerate Fermi system. At an extremely low, as yet unknown, temperature the diluted ^{3}He is also predicted to undergo a transition to the superfluid phase. The possibility of the discovery of such transition to an unprecedented system of two different intermixed superfluids is a major motivation of past and current research on dilute helium mixtures at ever lower temperatures. In this field, as well as helium research in general, various kinds of immersed mechanical oscillators have been widely used to probe the properties of the fluid under investigation. In this article we present results obtained by two types of such oscillators, vibrating metal wires and quartz tuning forks, in three experiments.

Vibrating wires have been a standard instrument of helium research for decades, but their behavior in helium mixtures is still not fully understood, in particular at the very lowest temperatures, that is, in the ballistic regime of the diluted ^{3}He that interacts with the wire. In the first experiment discussed in this article, helium mixtures were cooled deep into the ballistic regime, to temperatures of order < 0.1 mK, by means of nuclear demagnetization of copper. The mixture was probed by vibrating wires in small sample cavities embedded inside blocks of the copper coolant.

The second experiment was the first sub-millikelvin realization of adiabatic melting of ^{4}He in presence of superfluid ^{3}He, a method for cooling helium mixture through an internal process. This new approach to the problem of reaching ultra-low temperatures in helium mixtures has the advantage of avoiding the Kapitza thermal resistance barrier that limits cooling by any external refrigerant. In the adiabatic melting experiment, we employed two vibrating wires to probe pure ^{3}He, both superfluid and normal, and helium mixtures. Because of the cooling method, these vibrating wire measurements were done at the highest pressure at which liquid helium mixture exists, the melting pressure of ^{4}He in saturated helium mixture.

In the third experiment we studied, among other things, the prospects of using the quartz tuning fork, an oscillating probe relatively new to helium research, for our purposes. The fork proved a fast and accurate detector of the state of a helium mixture or pure ^{3}He despite the lack of a satisfactory analytical description of its response as a function of the properties of the fluid. Its sensitivity to the mass density of the surrounding medium, and thus to the ^{3}He concentration of helium mixture, enabled us to collect data on the critical supersaturation of the mixture, the limit by which the saturation concentration can be exceeded before spontaneous phase separation occurs.

Besides detecting the viscous damping and counterflow inertia as by vibrating wires, the tuning fork was found to excite and sense second sound, or concentration waves, in the helium mixture. This was seen in the vibration amplitude exercised by the fork as a multitude of sharp anomalies, to which the only plausible interpretation is that at certain wavelengths of second sound, there are resonant modes that increase greatly the transfer of energy. The tuning fork is sensitive to this phenomenon because at its resonance frequency, 32 kHz, the wavelength of second sound coincides with the dimensions of the fork and its cylindrical container.

Before presenting the experimental results from our measurements, we briefly discuss various descriptions upon the effect of a surrounding fluid on an oscillating vibrat-

ing wire. The theoretical work is later compared with experimental data.

2 Theory of vibrating wire

A typical vibrating wire resonator is semi-circular in shape, with loop diameter at least two orders of magnitude larger than the wire thickness, so that the wire can be treated as an infinitely long straight cylinder performing transverse oscillation. The effect of surrounding viscous fluid on such an object was solved exactly by Stokes [1], with the boundary condition that fluid velocity is zero at the cylinder surface. However, in pure ^{3}He and in the ^{3}He component of dilute helium mixtures this treatment is not valid at low enough temperatures because the mean free path of ^{3}He quasiparticles, l, becomes significant in comparison with the radius of the cylinder. The mean free path increases with lowering temperature as T^{-2} because of the Pauli exclusion rule limiting the scattering of the fermionic ^{3}He quasiparticles. According to Ref. [2], in helium mixtures the temperature dependence is roughly $l = 0.2\,\mathrm{mm}(T/\mathrm{mK})^{-2}$ at concentrations ranging from 1% to 9.5%. As the typical thickness of a vibrating wire is of the order of 0.1 mm, l exceeds the size of the oscillating object below 1 mK. In the temperature range where l is already significant but still below the size of the oscillator, a phenomenon called "slip" arises; there are a few published works on analytical corrections to the hydrodynamic solution of Stokes that take this into account [3, 4, 5]. At still lower temperatures, even the slip corrections become invalid as the fluid no longer behaves like a viscous continuum but rather like a gas of ballistic particles scattering from the surface of the oscillator.

2.1 Hydrodynamic approach

The equation of motion for the displacement $\mathbf{y}$ of a cylindrical body can be written as

$$A\rho_w\ddot{\mathbf{y}} + A\rho_w\omega_v^2\mathbf{y} = \mathbf{F}_e e^{-i\omega t} + \mathbf{F}_h, \tag{1}$$

with A the cross-sectional area and ρ_w the density of the cylinder, ω_v the resonance frequency in vacuum, and $\mathbf{F}_e$ the amplitude of a periodic excitation force. Following the notation of Stokes, the hydrodynamic force $\mathbf{F}_h$ on a cylinder oscillating at angular frequency ω in a viscous, incompressible fluid with density ρ is

$$\mathbf{F}_h = A\rho\omega^2\mathbf{y}(k + ik'), \tag{2}$$

where k and k' are dimensionless reals. It is illustrative to compare different oscillators in terms of these two numbers; therefore, we will next show how to determine them from the measured response of an oscillator. The physical meaning of k and k' becomes apparent when we use the time derivatives of a periodic solution $\mathbf{y} = \mathbf{y}_0\exp(-i\omega t)$ to express the equation of motion (1) as

$$A\,(\rho_w + \rho k)\,\ddot{\mathbf{y}} = \mathbf{F}_e e^{-i\omega t} - A\rho\,\omega k'\dot{\mathbf{y}} - A\rho_w\omega_v^2\mathbf{y}. \tag{3}$$

This form shows that the real part of the hydrodynamic force contributes to the inertia of the oscillator, whereas the imaginary part describes linear damping. When the fluid is a mixture of superfluid and normal fluid, like a dilute mixture of ^{3}He in ^{4}He, ρ in the damping term is replaced by ρ_n, the density of the normal component (calculated from the effective mass), and in the inertia term, ρk becomes $\rho_s + \rho_n k$, where ρ_s is

the density of the superfluid. Now, it is straightforward to show that the wire has a resonance frequency

$$\omega_r = \omega_v \left(\frac{\rho_w + \rho_s + \rho_n k}{\rho_w} \right)^{-1/2}. \tag{4}$$

In the limit of zero viscosity where the normal component exhibits ideal potential flow, k approaches unity. The limiting value of the resonance frequency in this ideal fluid limit, ω_i, is easy to determine from the measured data, gives a natural reference point for comparing resonance frequencies at finite viscosities, and can be used to cancel ρ_s from the treatment. Therefore, it is useful to express the resonance frequency in the form

$$\omega_r = \omega_v \left(\left(\frac{\omega_v}{\omega_i} \right)^2 + \frac{\rho_n}{\rho_w}(k-1) \right)^{-1/2}, \tag{5}$$

which allows more accurate calculation of k from a measured frequency than (4), because in practice ω_i deviates slightly from the theoretical value.

The oscillation of the wire is observed by measuring the induced voltage, proportional to the velocity of the wire, whose phase vector is $-i\omega \mathbf{y}_0 = \mathbf{v}_0$. On the grounds of (3) this depends on frequency as

$$\mathbf{v}_0 = \frac{\mathbf{F}_e}{A\rho_n \omega k'} \frac{1 + i\frac{\rho_w+\rho_s+\rho_n k}{\rho_n \omega^2 k'} \left(\omega^2 - \omega_r^2 \right)}{1 + \left(\frac{\rho_w+\rho_s+\rho_n k}{\rho_n \omega^2 k'} \left(\omega^2 - \omega_r^2 \right) \right)^2}. \tag{6}$$

Provided that the oscillator has a quality factor $Q \gg 1$, it is justified to approximate $\omega^2 - \omega_r^2 \approx 2\omega_r(\omega - \omega_r)$ and $\omega \approx \omega_r$ in the frequency range where the amplitude differs significantly from zero in comparison with its maximum. By these approximations and the definition

$$\Delta\omega_2 = \frac{\rho_n \omega_r k'}{\rho_w + \rho_s + \rho_n k} = \frac{\rho_n}{\rho_w} \left(\frac{\omega_r}{\omega_v} \right)^2 \omega_r k', \tag{7}$$

Eq. (6) becomes

$$\mathbf{v}_0 = \frac{\mathbf{F}_e}{A\rho_n \omega_r k'} \frac{1 + 2i\frac{\omega-\omega_r}{\Delta\omega_2}}{1 + \left(2\frac{\omega-\omega_r}{\Delta\omega_2} \right)^2}, \tag{8}$$

which represents a Lorentzian peak centered at ω_r and having a "full width at half maximum" equal to $\Delta\omega_2$. To summarize, the formulae for calculating the Stokes' parameters from the measured resonance characteristics are

$$k = 1 + \frac{\rho_w}{\rho_n} \omega_v^2 \left(\omega_r^{-2} - \omega_i^{-2} \right) \tag{9}$$

$$k' = \frac{\Delta\omega_2 \rho_w}{\omega_r \rho_n} \left(\frac{\omega_v}{\omega_r} \right)^2. \tag{10}$$

The solution provided by Stokes for calculating k and k' reads

$$k + ik' = 1 - \frac{4}{qa} \frac{H_1^{(1)}(qa)}{H_0^{(1)}(qa)}, \tag{11}$$

where $H_n^{(1)}$ are Hankel functions of the first kind and a is the radius of the wire. The symbol q is shorthand for $(1+i)/\delta$, where δ is the viscous penetration depth

$$\delta = \sqrt{\frac{2\eta}{\rho\omega}}, \tag{12}$$

a function of the two relevant properties of the fluid, density ρ and viscosity η. Thus, k and k' are functions of a single real variable δ/a, which means that the Stokes' solution determines a unique curve on the (k,k')-plane, parameterized by properties of the fluid and the oscillating cylinder. Although well known to be inadequate in pure or diluted ^{3}He, it is an illustrative reference curve.

To take the effect of slip into account, Højgaard Jensen *et al.*[3] present an improved formula equivalent to

$$k + ik' = 1 + \frac{4}{qa}\frac{\gamma(qa)}{1-\beta qa\gamma(qa)}, \tag{13}$$

where the function γ is defined

$$\gamma(z) = -\frac{H_1^{(1)}(z)}{H_0^{(1)}(z)} \tag{14}$$

and β is a function of the ratio of slip length ζ and wire radius a. The physical meaning of the slip length is that the tangential fluid velocity extrapolates linearly to zero at that distance inside the solid surface, and it is of the order of the mean free path l of fluid particles. Højgaard Jensen *et al.* estimate $\zeta = 0.579l$ and propose $\beta = \zeta/(\zeta + a)$, later shown to be valid only for $\zeta \ll a$ because of the curvature of the surface of the wire [6]. Guénault *et al.* [7] achieve best fit to their data by using the viscous mean free path as l to define

$$\beta = \frac{0.579l}{a}\sqrt{\frac{1+10\alpha^2 l/a}{1+10l/a}} \tag{15}$$

and assigning $\alpha = 2.3$. This is an empirical formula based on ideas of Carless, Hall, and Hook, who suggest that β is linear in l/a at the limit of both small and large l, but the proportionality factor increases in the intermediate region from the ζ/l of Højgaard Jensen *et al.* by a factor that lies between 2 and 3 [8].

A more recent analytical work of Bowley and Owers-Bradley (B&O-B) [5], and experimental results by Perisanu and Vermeulen [9], present a more sophisticated description of the problem. They calculate the slip effect directly in the correct cylindrical geometry (instead of applying a result for a planar surface) and take into account an enhancement of the slip length by specular scattering of quasiparticles from the wire surface. The degree of specularity of scattering is characterized by a parameter s, ranging from purely diffuse at $s = 0$ to purely specular at $s = 1$. The validity of the theory is limited to short mean free paths (the authors give a condition $l < a/10$), mostly specular scattering (s not much less than 1), and frequencies and wire radii so small in comparison with the Fermi velocity of quasiparticles that $a\omega/v_{\mathrm{F}} \ll 1$.

In both theories attempting to correct the Stokes' solution for the effect of slip, the resulting effective Stokes' parameter can be expressed as a function of two ratios, δ/a and l/a. These two are connected in a simple manner, because the viscosity of a normal Fermi liquid with Fermi momentum p_F obeys $\eta = np_F l/5$ which, together with Eq. (12), implies

$$\frac{l}{a} = \frac{5a\rho_n\omega}{2np_F}\left(\frac{\delta}{a}\right)^2. \tag{16}$$

The coefficient can also be expressed as $5a\omega/(2v_{\mathrm{F}})$, and it differs from the parameter $\Phi = 4i\rho\omega a/(3n_3p_F)$ of B&O-B just by a constant factor of $-\frac{15}{8}i$, and is in principle known.

2.2 Ballistic regime

Whereas the slip corrections extend the range of applicability of the hydrodynamical solution towards lower temperatures, there is currently no analytical description of the damping force in the truly ballistic temperature regime or in the transition regime where the mean free path is comparable to the wire diameter. It is, however, possible to treat analytically the limit $l \to \infty$, or $T \to 0$. Then, the damping force results from elastic collisions of quasiparticles with the wire and depends on the nature of the scattering, the extreme cases being specular scattering if the wire surface is perfectly smooth, and diffuse scattering from a rough surface. According to Virtanen and Thuneberg [10], the damping forces per unit length of the wire in the cases of specular and diffuse scattering are

$$\mathbf{F}_{\text{spec}} = -\frac{3\pi}{4} a n_3 p_F \mathbf{u} \quad \text{and} \tag{17}$$

$$\mathbf{F}_{\text{diff}} = -\frac{43\pi}{48} a n_3 p_F \mathbf{u}, \tag{18}$$

the former also found by B&O-B [5]. Above, p_F is the Fermi momentum of the ^{3}He quasiparticles and n_3 the number density of ^{3}He atoms. These results apply to a wire in an unbounded volume of helium; in reality, the experimental volume is finite and scattering from its walls has to be taken into account. Therefore, Virtanen and Thuneberg have more recently considered a wire in the middle of a cylindrical container and found an increase in the damping force in comparison with the unbounded case [11].

According to the equations above, the force exerted by the ^{3}He quasiparticles in the ballistic limit is in phase with the velocity of the wire, in other words, it is a pure damping force not contributing to the inertia of the wire. Thus, one would expect that the ballistic limit of the resonance frequency is determined by the density of the superfluid ^{4}He component, corresponding to $k = 0$ in the hydrodynamic approach. However, both our experimental results and numerical calculations of Virtanen and Thuneberg [12] show that in the ballistic limit, the resonance frequency actually reaches an even higher value, indicating that not only the ^{3}He component but also a fraction of the ^{4}He decouples from the wire as a result of interactions between the two components. Theoretical work on this effect is still in process.

2.3 Superfluid ^{3}He

Pure ^{3}He below its superfluidity transition temperature (T_c) is a mixture of a superfluid and normal liquid, with the important difference from the dilute helium mixture that the proportions of the components depend on temperature so that at T_c there is only normal liquid and at $T = 0$ all ^{3}He is superfluid. At temperatures only slightly below T_c the damping of a vibrating wire in ^{3}He has a complicated temperature dependence discussed, for example, in Ref. [8]. However, in the zero-temperature limit, two approximations are valid that lead to a simple functional form [13]. First, like in the case of mixtures discussed above, the mean free path of quasiparticles (excitations of the normal component) exceeds the dimensions of typical experimental devices, bringing the system to the ballistic regime. Then, the damping force obeys

$$\mathbf{F} = -A n_3 p_F a \mathbf{u} \sqrt{Y_0 Y_2}, \tag{19}$$

where Y_0 and Y_2 are Yosida functions determining the normal fluid density, and A a constant of the order 2. As the second simplifying approximation, below about 0.4 T_c

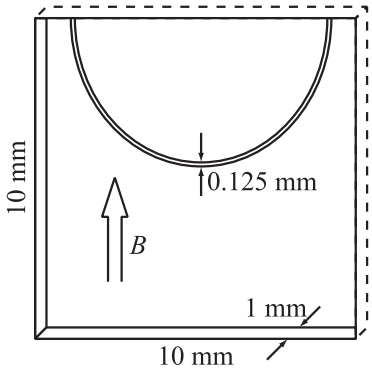

Figure 1: Vibrating wire in the sample cavity inside a block of copper nuclear coolant.

the square root of the two Yosida functions is proportional to $\exp(-\Delta/k_BT)$, where Δ is the superfluid energy gap. Since all other factors are independent of temperature, the resonance width follows a law of the same form:

$$\Delta\omega_2 \propto e^{-\frac{\Delta}{k_BT}}. \tag{20}$$

In our experiment on cooling mixtures by adiabatic melting of ^{4}He in superfluid ^{3}He, a vibrating wire was used for thermometry of ^{3}He well below 1 mK, so this limiting behavior could be expected.

3 Experiments

3.1 Demagnetization cooling

The conventional method to cool helium (or any other condensed matter) sample below a few mK, the minimum temperature practically achievable by a dilution refrigerator, is adiabatic demagnetization of copper nuclei. In a decent nuclear demagnetization cryostat, nuclear temperatures of tens of μK can routinely be reached, but the minimum temperature of any other system, even of the conduction electrons of the nuclear stage itself, is kept at a somewhat higher level because the thermal coupling to the cold nuclei weakens towards low temperatures. For helium liquids the weakening is especially rapid due to the thermal Kapitza resistance at the boundary between solid and liquid; there is said to be a "Kapitza barrier" at about 100 μK, preventing further cooling.

In our nuclear demagnetization cooling experiment on helium mixtures, we pushed the capability of this cooling method to the limit in an experimental setup with small sample volumes inside Cu blocks in a nested Lancaster-type cell. One of the three sample volumes is shown in Fig. 1; it contains a semicircular vibrating wire made of ∅ 125 μm Ta wire and is surrounded from all sides by sintered Ag powder on the surfaces of blocks of Cu. The magnetic field B is produced by the demagnetization magnet that embeds the whole experimental cell.

We used an advanced SQUID circuit for exciting and detecting the vibrating wire oscillation [14]. The sensitivity was so high that the oscillation amplitude could be kept at tens of nanometers. The experimental output, the frequency and width of the wire

resonance, were determined by first correcting a measured spectrum for frequency-dependent gain and phase and then fitting the theoretical resonance curve to the data. As only one SQUID was available for this purpose at the start of the experiment, we chose one of the three vibrating wires and used that throughout the experiment; another SQUID was added before measurements at elevated pressures so that during the latter half of the experiment, we also got data from another wire.

To avoid unnecessary heat loads, no other measuring devices besides the vibrating wires were installed in the cell. Therefore, direct measurement of the temperature of the cell was possible only down to about 3 mK by thermometers connected to the mixing chamber of the dilution refrigerator. By a thermal model of the cell, based on its physical structure, thermal resistances measured in the millikelvin regime, and qualitative features of the behavior at the lowest temperatures, we have estimated that the minimum temperatures of our mixture samples were between 70 and 90 μK [15]. At this temperature range, the mean free path of ^{3}He quasiparticles in the mixture is already over 2 cm, twice the largest dimension of the sample cavity. Thus, the ballistic regime was reached in the experiment, with respect to not just the size of the wire but also to the size of the liquid volume.

We experimented with six different mixtures, gradually increasing the ^{3}He concentration. The first four mixtures were studied at the saturated vapor pressure (SVP); their concentrations were 1.8%, 3.6%, 5.6%, and 6.6%, the saturation concentration at the low-pressure limit. In the experiments on the last two mixtures, 7.0% and 9.5%, pressure was raised to 1.02 MPa, reaching the maximum concentration in the zero-temperature limit. The concentration values are based on bookkeeping of the amounts of pure isotopes in the room-temperature gas mixture.

Figure 2 shows the resonance widths in the four SVP measurements as a function of temperature in the range where the thermometers of the dilution refrigerator could be used. The Lancaster slip formalism has been applied to produce the corresponding theoretical curves. In the calculation we used wire density 16.7 g/cm^3, ^{4}He molar volumes reported by Tanaka *et al.* [16], α's in the molar volume of the mixture by Watson *et al.* [17], and effective masses of ^{3}He according to Krotscheck *et al.* [18]. The viscosity of the ^{3}He component was modeled by a function of the form

$$\eta = c_2 T^{-2} + c_1 T^{-1} + c_0, \tag{21}$$

with the coefficients used as fitting parameters and listed in Table 1. The T^{-2} term, dominant at the lowest temperatures, is characteristic of a degenerate Fermi system, and the two others are needed to describe the behavior at higher temperatures. Mainly c_2 is of interest—it is the quantity ηT^2 usually referred to in works on the viscosity of dilute or pure normal ^{3}He in the mK regime. The values now obtained will shortly be compared with earlier results.

Figures 3 and 4 present the data from the two vibrating wires employed, plotting resonance width versus the resonance frequency to avoid the difficulty of thermometry

Table 1: Coefficients for calculating mixture viscosity at SVP

$x_3(\%)$	c_2 (mPas·mK^2)	c_1 (mPas·mK)	c_0 (mPas)
1.8	4.2	0	0.008
3.6	13	0.2	0.007
5.6	22	0.45	0.0025
6.6	28	0.5	0.0035

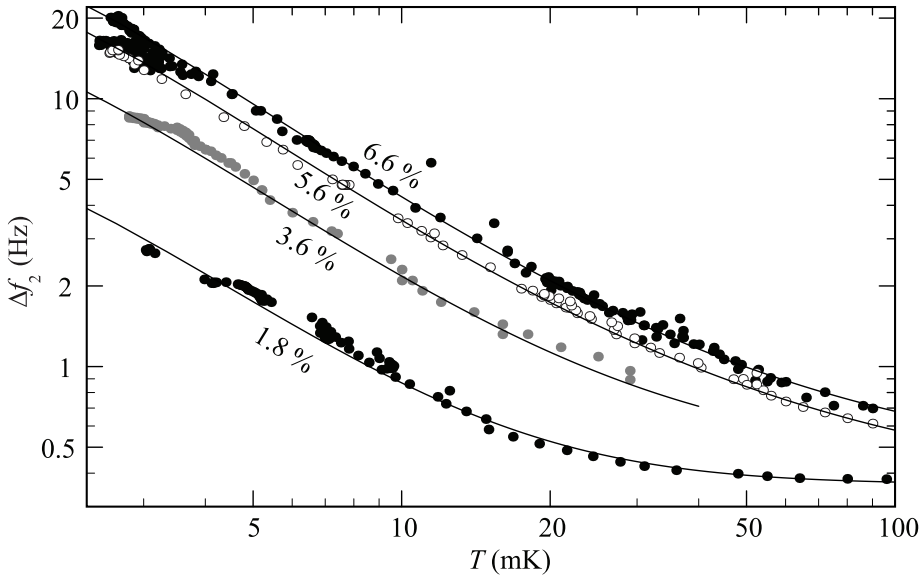

Figure 2: Resonance width of wire 1 as a function of temperature with four concentrations at SVP together with corresponding calculated curves.

of the sample at sub-millikelvin temperatures. Some of these data have already been published in Refs. [19] and [20]. The horizontal dashed lines indicate the theoretical resonance widths in the ballistic limit ($T = 0$) for each concentration: the values for specular scattering are shown by long dashes, and the values for diffuse scattering, somewhat higher than the corresponding specular values, by short dashes.

The low-temperature ends of the data from wire 1 at SVP systematically lie between the specular and diffusive limits. However, the experiments at 1.02 MPa produced resonance widths remaining clearly below the specular value. This may indicate that the ballistic limit was not quite as complete in the pressurized cell. A plausible reason for this is that under pressure, the filling line of the cell was full of liquid and formed a significant conductor of heat between the cell and warmer parts of the setup, limiting the lowest attained temperatures.

Figures 5, 6, and 7 present the vibrating wire data converted to effective Stokes parameters by Eqs. (9) and (10), and theoretical curves given by the Stokes solution, the Lancaster formula, and the theory of B&O-B with four values of specularity s: 1, 0.8, 0.6, and 0.4. No fitting has been done as all parameters of the curves are from literature. Note that as B&O-B neglect diffusive scattering in their treatment, the curves corresponding to the lowest values of s are merely suggestive.

The lower parts of the plots represent the hydrodynamic regime where the data can be compared with the theoretical curves. In the data from wire 1, there is a clear trend with increasing concentration: the observed behavior changes from a striking agreement with the Lancaster curve towards the B&O-B curves for mainly specular scattering. In accord with a remark by Perisanu and Vermeulen on König's work with a similar Ta wire [21], the data from saturated mixture at SVP suggests $s \approx 0.5$, although that value is already beyond the validity range of B&O-B theory.

Let us also consider the ballistic regime, or the upper ends of the arcs of data points.

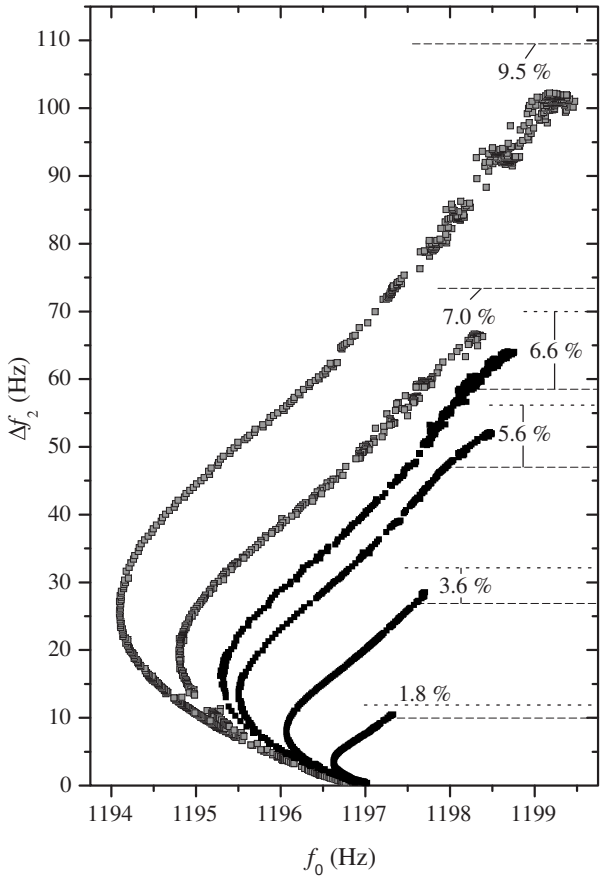

Figure 3: Data from wire 1 in six helium mixtures. Black symbols present measurements at SVP and gray symbols at 1.02 MPa. Dashed lines mark the theoretical $T = 0$ limits of the resonance width, long dashes for specular and short dashes for diffuse scattering.

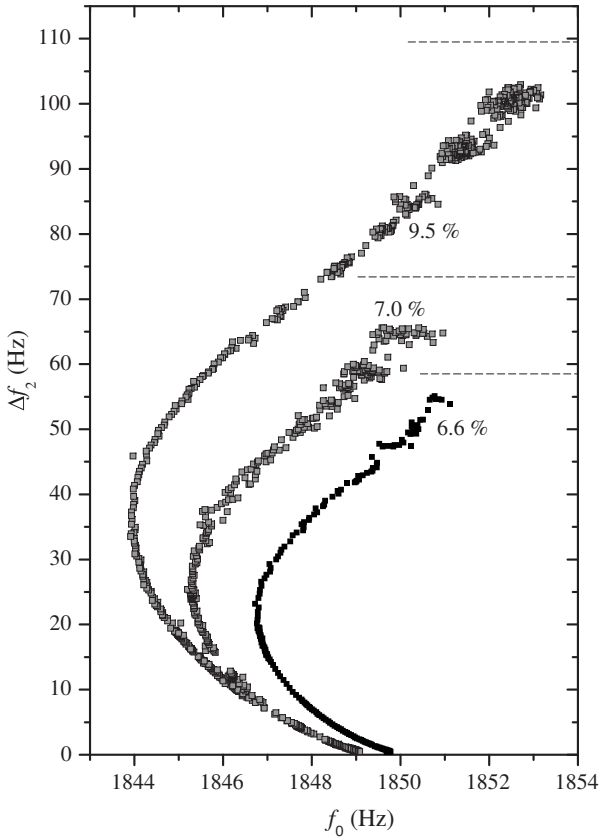

Figure 4: Data from wire 2 in three helium mixtures. Black symbols present measurements at SVP and gray symbols at 1.02 MPa. Dashed lines mark the theoretical $T = 0$ limits of the resonance width for specular scattering.

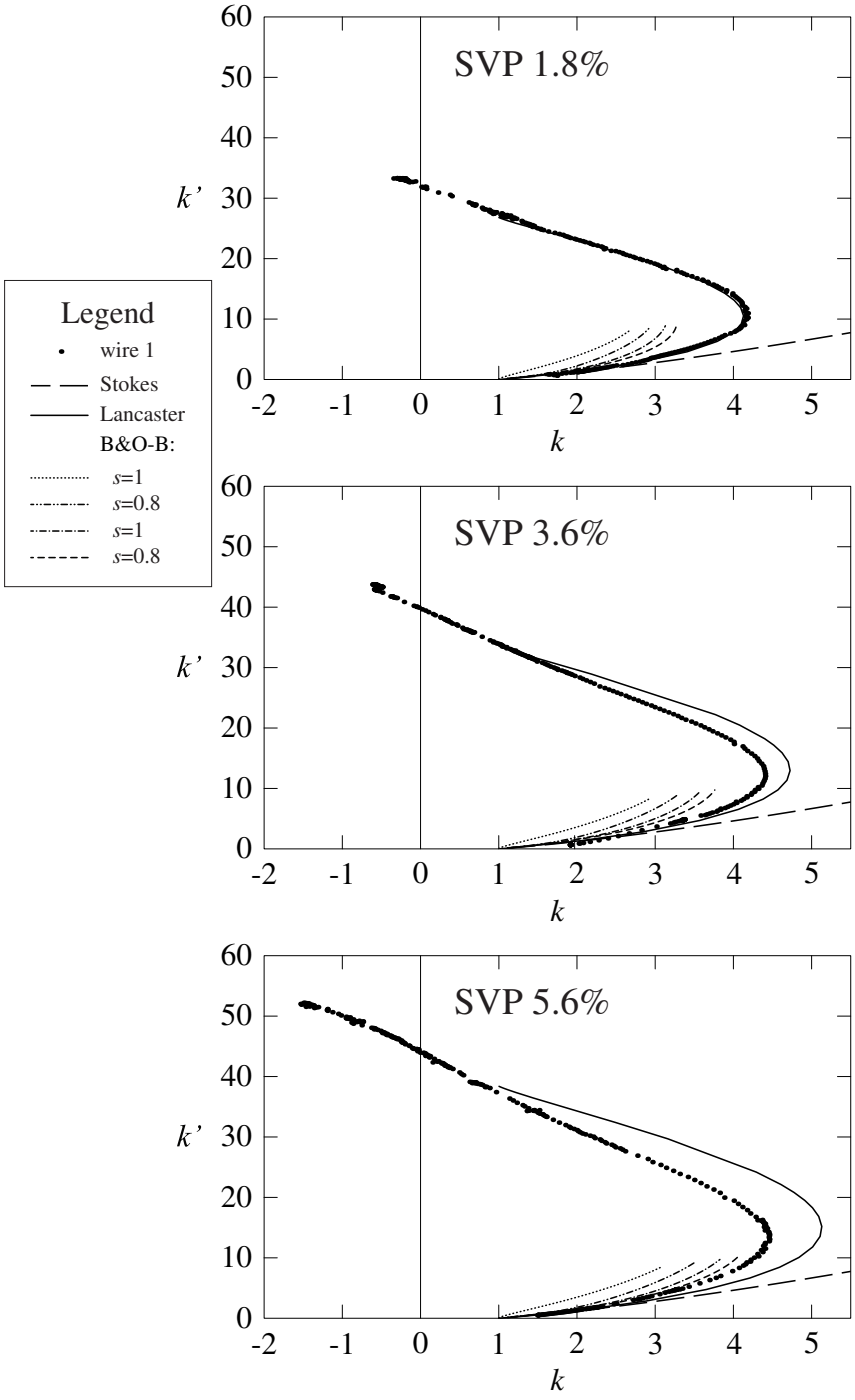

Figure 5: Effective Stokes parameters measured at SVP below saturation concentration, and curves calculated by Stokes' solution, Lancaster slip formula, and the theory by Bowley and Owers-Bradley.

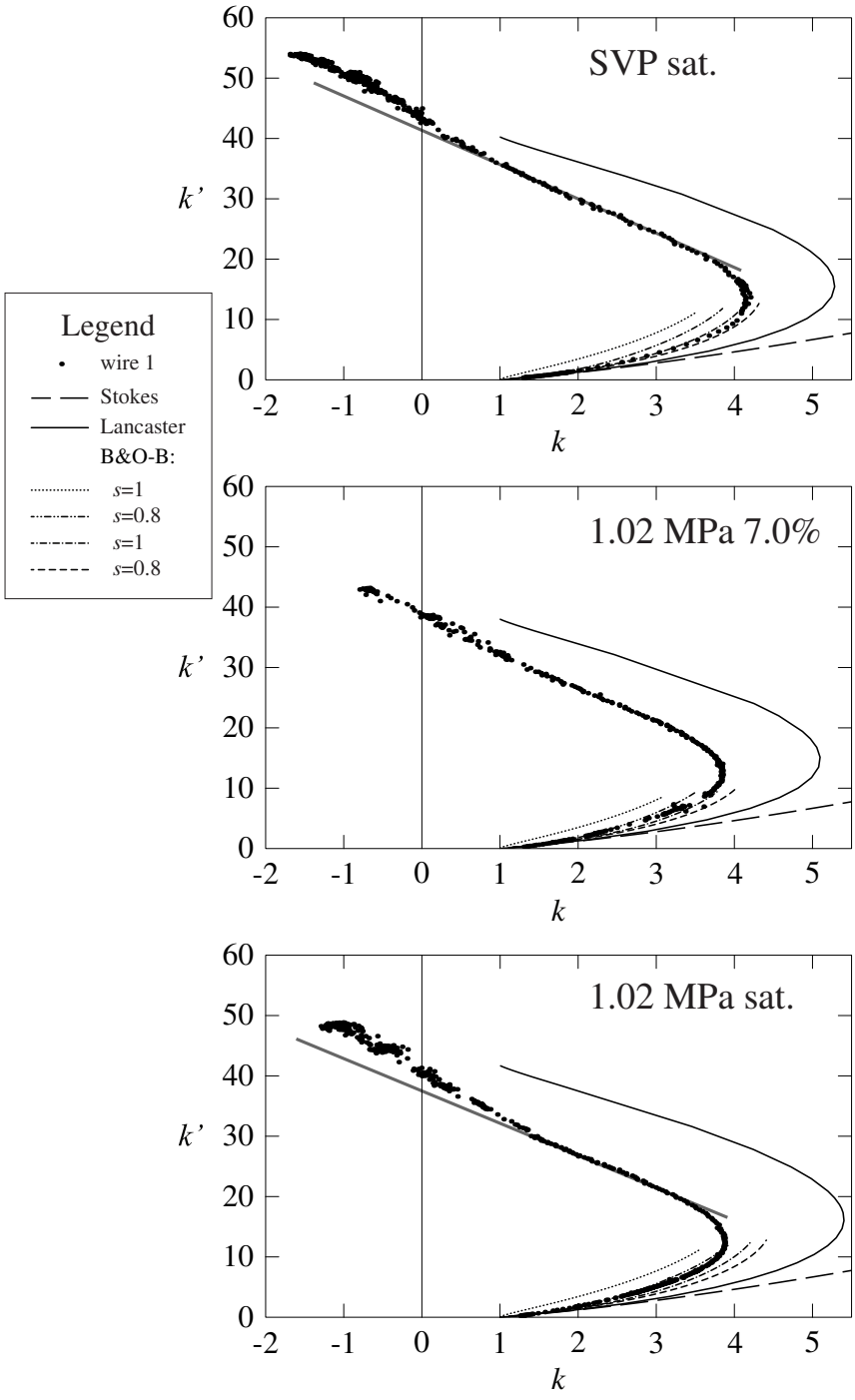

Figure 6: Effective Stokes parameters in saturated mixture at SVP and at 1.02 MPa in two concentrations. Calculated curves like in Fig. 5. The gray lines are guides to the eye.

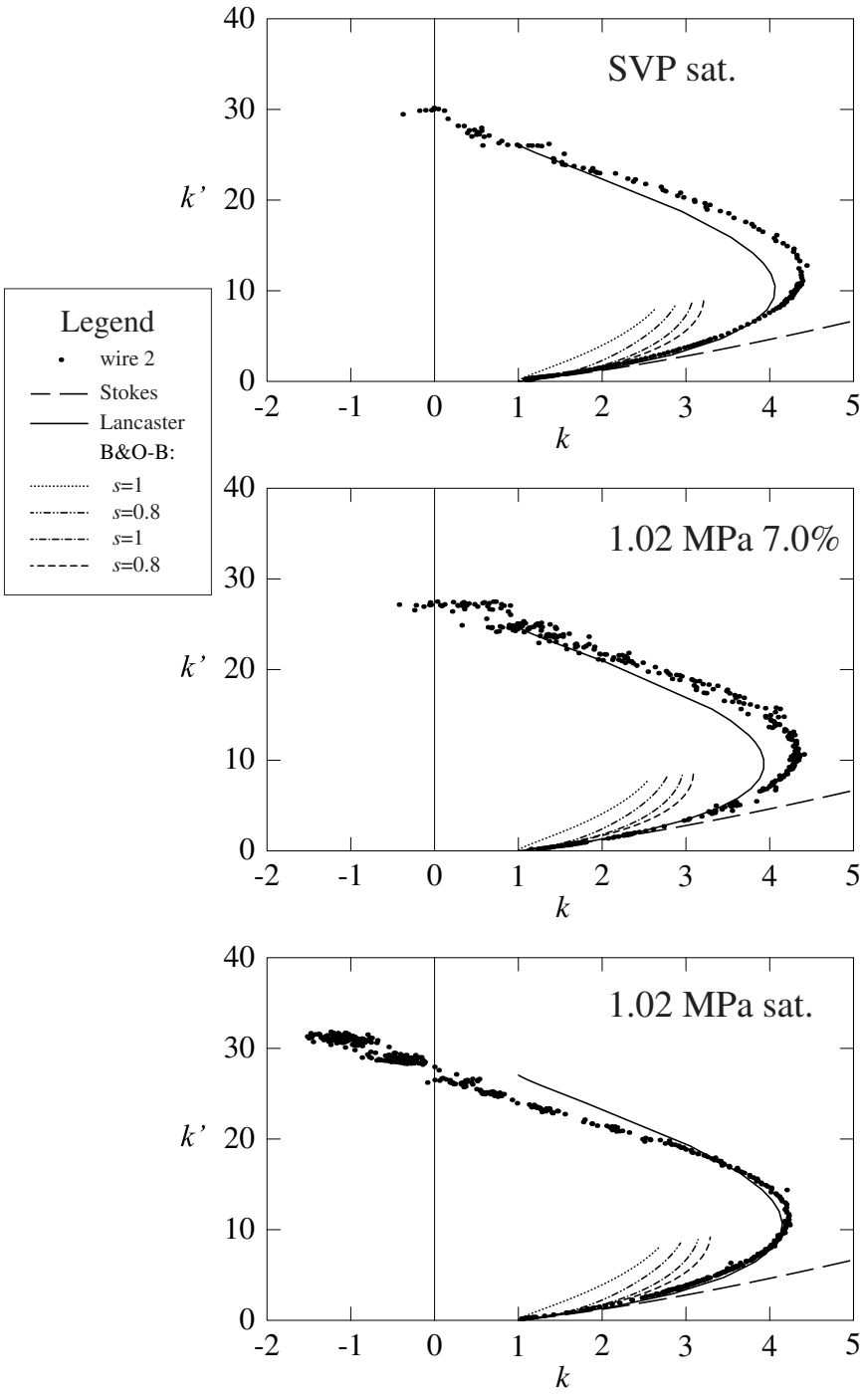

Figure 7: Effective Stokes parameters for wire 2. Calculated curves like in Fig. 5.

There, the major finding is that in each case, k reaches negative values, meaning that the hydrodynamic mass of the vibrating wire is reduced more than by the effective mass of the ^{3}He component. This is the unexpected but numerically reproducible observation already mentioned in Sec. 2.2. Another feature that the present theories do not reproduce is the gentle bend near the $k = 1$ point, emphasized on the top and bottom plots of Fig. 6 by straight gray lines drawn through a virtually linear part of the data. One explanation for this bend could be that it results from the mean free path of quasiparticles reaching the size of the sample cavity. Testing this hypothesis is challenging as it would require an experiment in a notably larger sample cavity with the same cooling capability.

3.2 Adiabatic melting

Adiabatic melting of ^{4}He in ^{3}He is a method of cooling liquid helium mixture by an internal process, thus avoiding the difficulty of efficiently coupling the sample to an external coolant at ultralow temperatures. Our experiment was the first realization of the method below 1 mK in superfluid ^{3}He; details of the experimental setup and cooling results are presented in Ref. [22].

The principle of the cooling method is the following. The helium isotopes are first separated by pressurizing a liquid helium mixture to the pressure at which a solid phase appears; at sufficiently low temperature, below some 50 mK, a crystal of essentially pure ^{4}He is formed, and all ^{3}He remains in the liquid phase. Ideally, the sample eventually consists of two isotopically pure phases: solid ^{4}He and liquid ^{3}He. The second step is to precool the separated sample by a nuclear demagnetization stage to a temperature where the liquid ^{3}He phase is deep in the superfluid state; about 0.5 mK is low enough and still relatively easy to reach despite the inevitable thermal resistance between the nuclear stage and the helium sample. After precooling, pressure is lowered so that ^{4}He starts to melt and a liquid mixture of the isotopes appears again. Because of the extremely small entropy content of both the pure phases in comparison with mixture at the same temperature, the mixture being formed is significantly colder than the initial temperature as long as the process is adiabatic. To cope with this, our experimental cell was made very rigid, and (instead of a bellows or other variable volume common in other experiments on high-pressure helium) the pressure was controlled by inserting and extracting superfluid ^{4}He through a superleak line. Because the sample is intended to cool below the temperature of the cell wall, the thermal contact between them has to be optimized so that it is sufficient for the precooling but not so strong that the cooling power of the melting process is wasted in cooling down the cell wall and the nuclear stage.

The three helium phases present during the adiabatic melting form a univariant system, where, for example, temperature determines uniquely the pressure and the concentration of the liquid mixture. In the zero-temperature limit, the equilibrium pressure of the three-phase system is 2.564 MPa and the ^{3}He concentration of the mixture about 8.1%.

3.2.1 Vibrating wires

For monitoring the state of the helium sample, two vibrating wires were installed inside the cell. They were placed horizontally one above the other, so that in a typical configuration, both liquid phases could be probed: the pure ^{3}He phase by the upper one and the mixture phase by the lower one—see Fig. 8. Since the experimental cell was

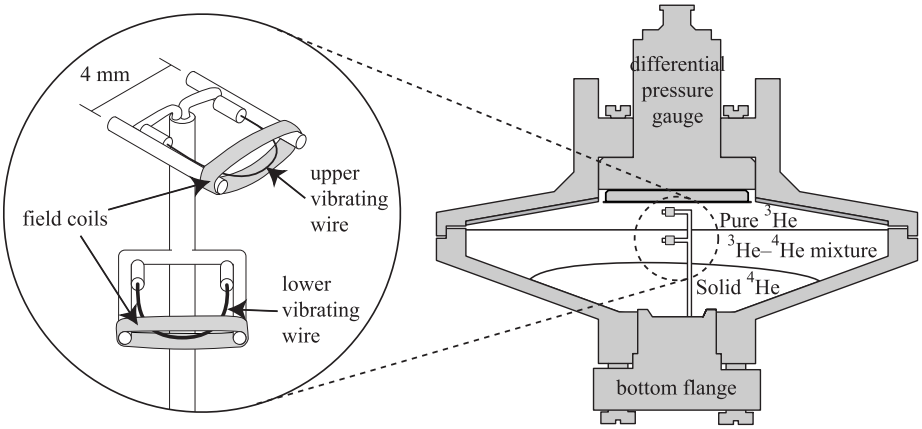

Figure 8: The double vibrating wire insert in the adiabatic melting experiment: a schematic perspective view and position in the cell.

not in an external magnetic field, the field necessary for the operation of the vibrating wires was produced locally by compact elongated coils, supported by the same post that held the vibrating wires in position. The supporting structure was made of CuNi tube and stood vertically on the bottom flange of the experimental cell.

As temperature decreases well below 1 mK in the adiabatic melting experiment, damping experienced by the wire in the dilute mixture approaches the ballistic upper limit, whereas in the superfluid pure ^{3}He, damping decreases rapidly according to Eq. (20). In both cases damping is due to ballistic quasiparticles, giving rise to a resonance width inversely proportional to the radius a and to the density ρ_w of the wire. In order to keep the resonance widths of the two vibrating wires within a measurable range, wire materials had to be chosen so that $a\rho_w$ was low for the upper wire and high for the lower wire. Therefore, the upper wire was made from the NbTi core of a single-filament superconducting wire with diameter 50 μm, and the lower wire from tantalum wire with diameter 125 μm. The density of the NbTi filament is not known precisely, but it is about 6 g/cm^3, clearly below the density of tantalum, 16.7 g/cm^3.

The density of the upper wire can be estimated using Eq. (4) in the form

$$\left(\frac{f_v}{f_r}\right)^2 - 1 = \frac{\rho_s}{\rho_w}, \tag{22}$$

with resonance frequency in vacuum, $f_r = f_v = 1071.5$ Hz, and values for superfluid ^{4}He at SVP ($f_r = 1057.55$ Hz, $\rho_s = 0.145$ g/cm^3) and at melting pressure ($f_r = 1055.27$ Hz, $\rho_s = 0.173$ g/cm^3). Linear fitting to these data implies wire density $\rho_w = 5.5$ g/cm^3.

3.2.2 Results

Figures 9 and 10 show the measured resonance widths of the lower and upper vibrating wires in the helium mixture of the three-phase system, respectively, and curves based on the Lancaster slip correction. For the effective mass of ^{3}He in the mixture we used a value 3 times the atomic mass; this is a quantity that has not been measured above

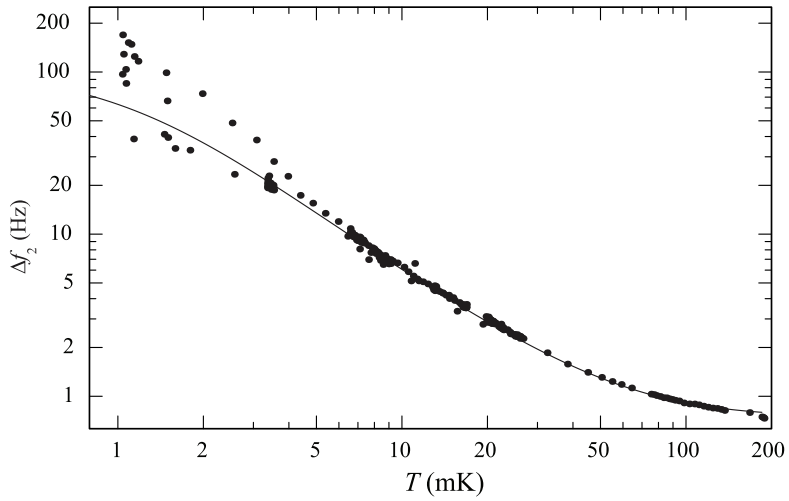

Figure 9: Resonance width of the lower (Ta) wire in saturated mixture at melting pressure, measured values and a calculated curve.

2 MPa, but the pressure dependence is regular enough for fair extrapolation. Also for the molar volume of the mixture, customarily expressed as $v_m = v_{40}(1+\alpha x)$ with v_{40} the molar volume of pure ^{4}He, α the BBP parameter after Bardeen, Baym, and Pines [23], and x the share of ^{3}He atoms in the mixture, we have to rely on extrapolated values $v_{40} = 23.2$ cm^3/mol and $\alpha = 0.165$. As the density of the lower wire, made of pure tantalum, is known beforehand, the data measured by it can be used to find an expression for the viscosity of the ^{3}He component in the saturated mixture. A good agreement between experiment and theory is achieved by letting the viscosity depend on temperature as

$$\eta = \left(2.6 \times 10^{-8} \left(\frac{T}{\mathrm{K}} \right)^{-2} + 5 \times 10^{-6} \right) \mathrm{Pa \cdot s}. \tag{23}$$

Then, by treating the less well known density of the upper wire as a fitting parameter, a value as low as 4 g/cm^3 has to be applied to produce the curve shown in Fig. 10.

The amount of ^{3}He in the cell was such that the pure ^{3}He phase, always floating on top, could only reach the upper wire. The measured resonance widths in pure ^{3}He are presented in Figs. 11 and 12, above and below the superfluid transition, respectively. In addition to experimental data, Figure 11 also shows two curves calculated by the Lancaster slip correction, corresponding to wire densities 4 g/cm^3, the value suggested by the mixture measurements, and 6 g/cm^3, which gives a good fit to this data and is also closer to the value estimated from the resonance frequencies in vacuum and superfluid ^{4}He. The viscosity of normal ^{3}He was calculated by

$$\eta = \left(\frac{1}{6.65(T/\mathrm{mK})^2 + 12.8} + 10^{-5} \right) \mathrm{Pa \cdot s}, \tag{24}$$

where the first term is based on an interpolation of data in Table I of Carless *et al.* [4], and the second, constant term was applied to reproduce the flattening of the dependence at high temperatures.

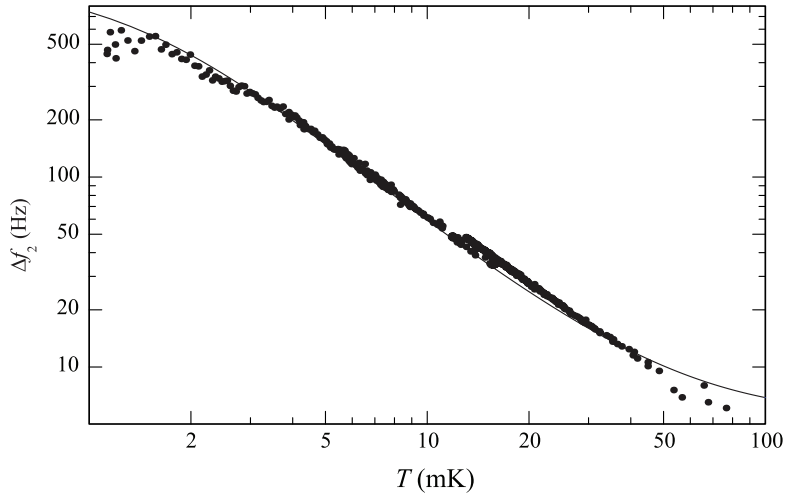

Figure 10: Resonance width of the upper (NbTi) wire in saturated mixture at melting pressure, measured values and a calculated curve.

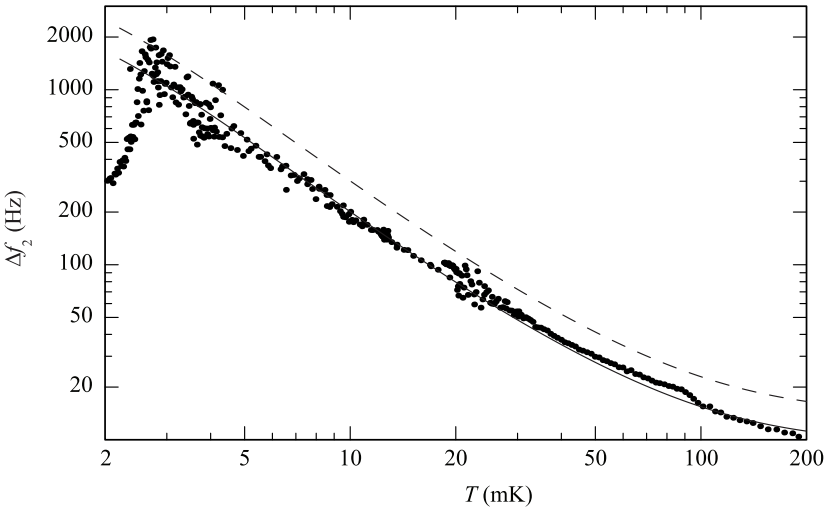

Figure 11: Resonance width of the upper vibrating wire in normal pure ^{3}He, and calculated curves assuming wire densities 4 g/cm^3 (dashed line) and 6 g/cm^3 (solid line)

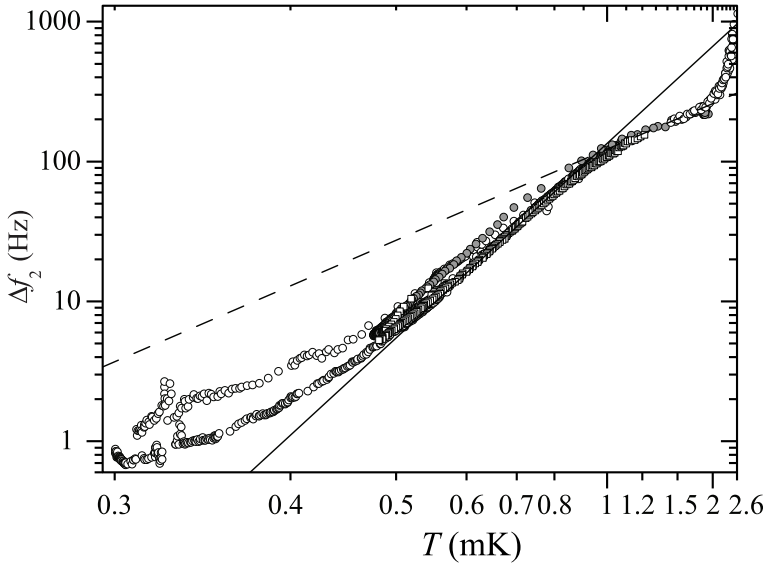

Figure 12: Resonance width of the upper vibrating wire in ^{3}He below the superfluid transition, and graphs of $550\exp(-1.5\,\mathrm{mK}/T)$ Hz (dashed) and $3300\exp(-3.2\,\mathrm{mK}/T)$ Hz (solid line). The temperature is that of the cell body measured by a Pt-NMR thermometer.

In Fig. 12, the width axis is logarithmic and the temperature axis is reciprocal, so that graphs of functions of the form given in Eq. (20) are straight lines. As expected, below 1 mK the data follows such a line down to about 0.5 mK, where the measured temperature of the cell wall probably starts to differ significantly from the liquid temperature. As the vacuum width of the upper wire was below 0.2 Hz, the observed linear low-temperature dependence can be assumed to be valid at least down to about 0.4 mK, and was used to indicate the temperatures reached by the adiabatic melting method and reported in Ref. [22]. The slope of the fitted line suggests $\Delta/k_B = 3.2$ mK, whereas according to theory, the energy gap in superfluid ^{3}He is larger than the BCS value $1.76\,T_c \approx 4.3$ mK; Todoshchenko *et al.* have observed behavior corresponding to $\Delta/k_B = 1.99\,T_c$ in their vibrating wire measurements at the melting pressure of ^{3}He [24].

Finally, Fig. 13 shows a plot of the low-temperature viscosity of dilute helium mixtures in terms of the quantity ηT^2, combining data of König and Pobell [2] and our vibrating wire results from the two experiments discussed so far. All low pressure data are well described by an empirical formula $\eta T^2 = x^{1.45} \cdot 1.48 \cdot 10^{-6}$ Pa s mK^2. Our result at melting pressure is consistent with the viscosity decreasing as a function of pressure, a matter of which König and Pobell could not draw a firm conclusion.

3.3 Quartz fork in helium

The third experiment covered in this report was built around some critical components of the previous adiabatic melting experiment for testing purposes. The setup was suit-

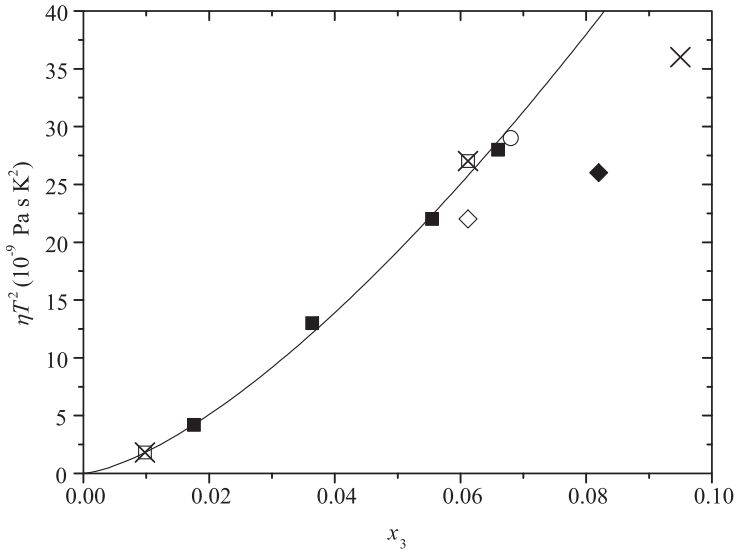

Figure 13: Values of ηT^2 of helium mixtures at different concentrations and pressures and an empirical power-law fit to the zero-pressure data. Our data at SVP (■) and melting pressure of saturated mixture (⧫). Data of König and Pobell [2] at SVP (□), 0.035 MPa (○), 0.97 MPa (×), and 1.94 MPa (◇).

able for various kinds of measurements on dilute helium mixtures and pure helium isotopes. A description of the setup and results on the solubility of ^{3}He in the dilute mixture over the complete range of pressures have been published in Ref. [25], and the melting pressure of helium mixture in the mK regime as a means of determining the osmotic pressure of the mixture will be treated in a forthcoming publication. Here we will present results on the behavior of an oscillating quartz tuning fork immersed in the helium sample. Figure 14 depicts the fork employed in our experiment. The cylindrical container, originally vacuum sealed, was left in place, but two holes (only one visible in the picture) were filed into it to allow helium in.

Quartz forks have already been successfully employed in low-temperature helium research, in a similar manner as vibrating wires and other mechanical oscillators, by a few other groups [26, 27]. This new tool has some apparent advantages in comparison with the vibrating wire: its operation is based on piezoelectricity instead of Lorentz force and magnetic induction, so that, firstly, magnetic field neither is needed nor affects the measurement, and secondly, the measured signal is more intense relative to excitation. Moreover, as quartz has a regular crystal structure, the physical properties of the fork do not vary below 1 K and are unaffected by changes of pressure within the range where liquid helium exists, and internal damping and thereby the vacuum resonance width are extremely low. A quartz tuning fork can be described as a linearly damped harmonic oscillator in a similar way presented for vibrating wires in Section 2.1, with the difference that as the output voltage is proportional to displacement instead of velocity, the (nearly) Lorentzian peak is observed in the quadrature component of the signal with respect to excitation.

The resonance frequency of a standard tuning fork, designed to respond at 2^{15} Hz $\approx$

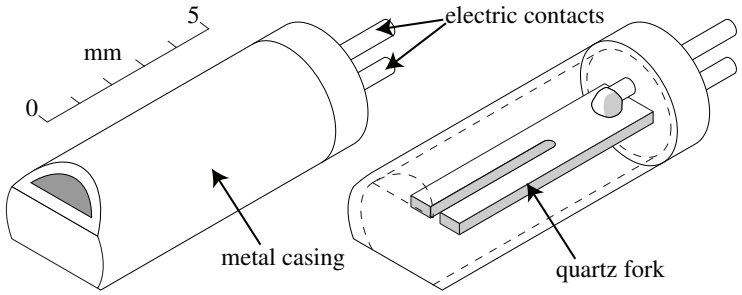

Figure 14: Quartz tuning fork employed in our helium mixture experiment, external and internal view.

32.8 kHz in vacuum at room temperature, is more than ten times higher than that of a typical vibrating wire. Therefore, the viscous penetration depth, defined by Eq. (12), is smaller than in the case of the wires by a factor of order four. On the other hand, the tines of available tuning forks are a couple of times thicker than wires usually used as oscillators. These two factors together imply that for a tuning fork immersed in a viscous fluid, the ratio of the size of the oscillator to the viscous penetration depth (denoted by a/δ in the theory of vibrating wires) is notably larger than for a vibrating wire. As a consequence, the ratio of the resonance width to the resonance frequency is smaller, in other words, the Q-value is higher. This is an advantage in highly viscous fluids, such as normal pure and diluted ^{3}He at mK temperatures, where the resonance width would otherwise become inconveniently high—consider, for example, the upper vibrating wire in our adiabatic melting experiment, whose resonance peak in pure ^{3}He close to T_c had a width comparable to the resonance frequency, was far from Lorentzian, and proved very difficult to extract from the frequency-dependent background resulting in poor measurement accuracy.

In addition to frequency and size, wires and forks also differ in terms of density. Quartz, of which tuning forks are made, has a density of 2.65 g/cm^3, notably smaller than densities of the metallic vibrating wires. Consequently, the relative change of the resonance frequency as a function of the density of the surrounding fluid is larger for tuning forks than for vibrating wires. On the other hand, even the highest densities of liquid helium phases are more than an order of magnitude smaller than that of quartz, so that the resonance frequency of a fork in helium varies within a convenient range of a few kilohertz below the vacuum value.

3.3.1 Single-frequency measurement

Like a vibrating wire, an immersed quartz tuning fork gives information on the surrounding fluid through the frequency and width of its mechanical resonance. In most of our fork measurements, we determined these variables by measuring the fork signal at a single frequency close to the resonance. This single-frequency method is much faster than recording entire spectra; we typically acquired a new data point in every two or three seconds, a sampling rate more than sufficient for most purposes.

Before the single-frequency method could be used, we had to record a calibration spectrum of the fork signal at stable conditions in order to determine the background offset and phase shift originating from the detection circuit, and the amplitude and

width of the resonance peak. The offset and phase were then used to extract the actual fork response from the measured signal for the single-frequency measurement. According to the solution of the equation of motion (1), the phase-corrected AC response, measured at frequency f, consists of two components

$$u_1(f) = \frac{C}{w}\left(1+\left(\frac{f^2-f_0^2}{wf}\right)^2\right)^{-1} \tag{25}$$

$$u_2(f) = \frac{C}{w}\,\frac{f^2-f_0^2}{wf}\left(1+\left(\frac{f^2-f_0^2}{wf}\right)^2\right)^{-1}, \tag{26}$$

where w and f_0 are the width and frequency of the resonance. C is essentially a constant provided that f and f_0 are limited to a narrow range of frequencies, which was ensured by measuring the calibration spectrum at or close to the conditions where the single-frequency method was to be applied. As $u_1(f_0) = C/w$, the constant C is simply the product of the width and amplitude of the peak, known from the spectrum measurement and proportional to the area of the peak. It is straightforward to solve w and f_0 from the equations above; a practical form of the solution that we used in our measurement is to first calculate w from just the signal and the constant C by

$$w = \frac{Cu_1}{u_1^2+u_2^2}, \tag{27}$$

and then f_0 by

$$f_0 = \sqrt{f\left(f - w\frac{u_2}{u_1}\right)}. \tag{28}$$

For maximal accuracy, the fork response should be measured as close to the resonance (the maximum of u_1 and zero of u_2) as possible, at least within the width of the resonance. To ensure this, we controlled the measurement by a computer program that set a new frequency after each measurement, either at the previous resonance frequency or at a value predicted by linear extrapolation from the two previous values. The latter mode is preferable when the resonance peak is narrow and changes frequency more or less regularly. On the other hand, if the resonance frequency varies in an unpredictable way, extrapolation is unfavorable as it may erroneously select the next measurement frequency so far away from the resonance that the program looses track of it altogether—this happened occasionally in our experiments, sometimes because an acoustic resonance of the surrounding liquid passed the fork resonance and the measurement algorithm started to follow that.

3.3.2 Results in mixtures

The experiment with the tuning fork was a long continuous cooling, started by filling the cell by pure ^{4}He, and proceeded by gradually replacing it by small doses of ^{3}He. Isotopes were exchanged by adding ^{3}He through a customary filling capillary while removing ^{4}He via a superleak line, with the cell usually at the saturated vapor pressure (SVP) and at 10 mK. The chosen temperature was easily maintained by our dilution refrigerator despite the heat load of the incoming warm ^{3}He, but also low enough so that the saturation concentration of the dilute helium mixture does not differ significantly from its zero-temperature value. Figure 15 shows how the width of the fork resonance

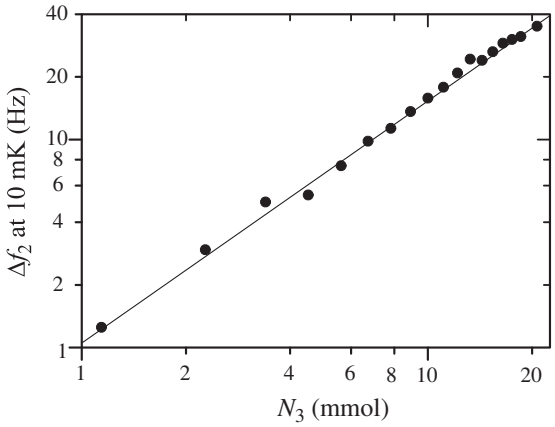

Figure 15: Resonance width of tuning fork at SVP and 10 mK as a function of the ^{3}He content of the cell up to the saturation limit. The linear fit represents a power law with exponent 1.164.

at the said conditions increased with the ^{3}He content of the cell. The data covers the whole concentration range up to the saturation limit of about 6.6 %, and follows a power law $\Delta f_2 \propto {N_3}^{1.164}$, presented by the straight line in the graph. The visible local deviations from the regular power-law behavior are most probably due to resonances of second sound in the mixture. A power law with an exponent somewhat above one is what one expects on the grounds of the theory for viscous damping on cylinders. Namely, by Eq. (7), the resonance width is, to the first order, proportional to $\rho_n k'$, where k' is, in turn, well approximated by $2\delta/a$ at small δ, and thus proportional to $\sqrt{\eta/\rho_n}$. On the basis of vibrating wire measurements, $\eta \propto {x_3}^{1.45}$, and because ρ_n, N_3, and x_3 are approximately proportional to each other in dilute mixtures, this reasoning results in $\Delta f_2 \propto {N_3}^{1.225}$.

Before reaching the saturation solubility of ^{3}He in the sample, we focused on measurements of the melting pressure of the mixtures, reported elsewhere, instead of systematically examining the dependence of the fork response on concentration, temperature, and pressure. Some fork data was, however, gathered at the chosen 10 mK reference temperature while changing the pressure between SVP and the melting pressure. Observed resonance widths in different mixtures are plotted as a function of pressure in Fig. 16 together with data for the saturated mixture. Because we controlled the pressure of the sample by adjusting the amount of ^{4}He in a constant volume, a given data set is not for a fixed concentration x_3 but for a fixed number density of ^{3}He.

The experiment entered a new phase when the ^{3}He content of the cell reached a value sufficient to saturate the mixture at low temperatures and pressures. We studied the pressure and temperature dependence of the saturation solubility, and also continued the melting pressure measurements. Figure 17 illustrates the domain in which the fork response varied, with arrows that indicate how changes in pressure, temperature, and concentration influenced the fork.

In principle, the resonance width data could be used to determine the saturation concentration at different pressures, but because of its strong temperature dependence, an independent means of accurate thermometry of the mixture would then be necessary.

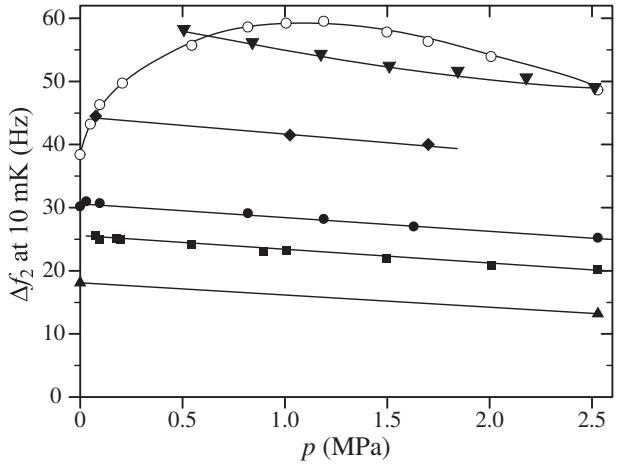

Figure 16: Resonance width of tuning fork in helium mixtures at 10 mK as a function of pressure. Each set of data is for a constant amount of ^{3}He in the cell: 11.1 mmol (▲), 14.3 mmol (■), 17.5 mmol (●), 21.1 mmol (♦), 29.7 mmol (▼), and saturated mixture (○). The lines are guides to the eye.

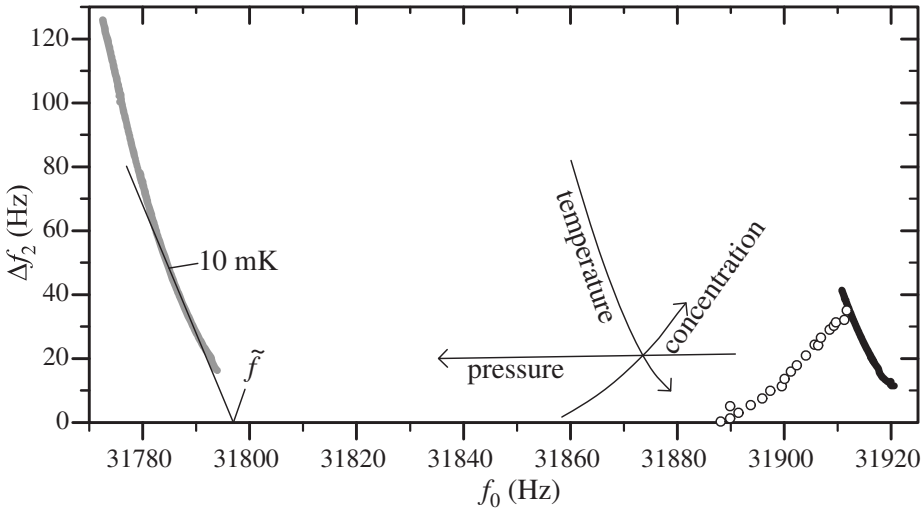

Figure 17: Variation of the tuning fork response with changes in the three variables defining the state of helium mixture. Experimental points for ^{3}He concentration range from zero to saturation at SVP and 10 mK (circles), temperature range from about 7 to 70 mK in saturated mixture at SVP (black), temperature range from about 1 to 35 mK in saturated mixture at melting pressure (gray). A line with slope -4 drawn through the melting pressure data illustrates the extrapolation of the resonance frequency to the zero-viscosity limit $\tilde{f}$.

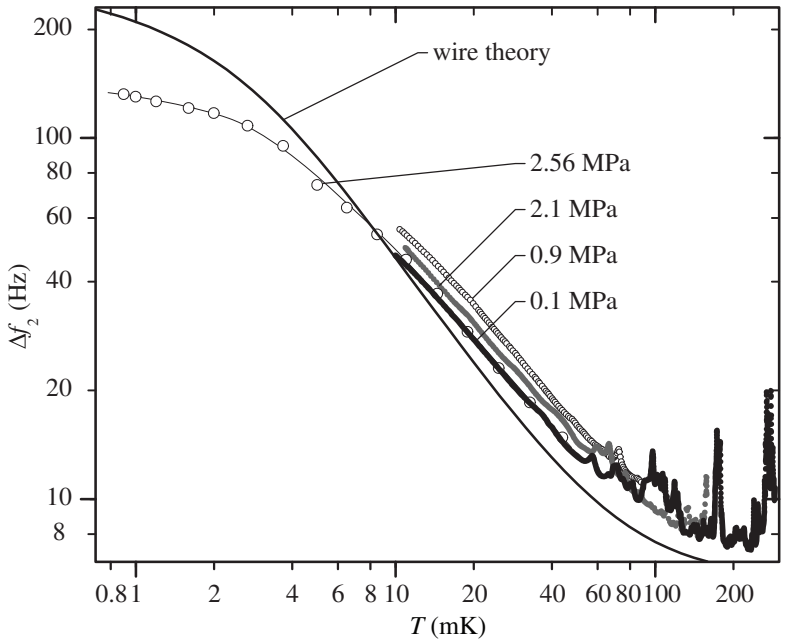

Figure 18: Resonance width of tuning fork in saturated mixture at pressures shown on the graph, and a calculated curve for a vibrating wire with radius $a = 0.15$ mm at 2.56 MPa.

To reduce the effect of temperature variations, we based our solubility measurements on the quantity $\tilde{f} = f_0 + \Delta f_2/4$, a projection to the frequency axis in the direction of the temperature dependence around 10 mK. When calculated from results taken at about that temperature, $\tilde{f}$ has very little temperature dependence while indicating clearly changes in concentration and pressure, the latter of which is readily measurable by an external pressure gauge.

Figure 18 presents the temperature dependence of the resonance width of the fork in saturated mixtures at four pressures. The data for the melting pressure, extending down to below 1 mK, were acquired during the only demagnetization cooling with this setup. Otherwise we rarely cooled the sample much below 10 mK. The theoretical curve in the graph has been calculated by the vibrating wire theory for a wire with a radius of 0.15 mm in saturated mixture at its melting pressure. In agreement with fork results of Clubb *et al*. [26], the temperature dependence in the hydrodynamic regime appears to have a lower slope than the approximately T^{-1} predicted by theory and demonstrated by vibrating wires. The pattern of sharp peaks that dominate the resonance width above about 50 mK is attributed to resonances of second sound in the mixture, a phenomenon discussed in the following section.

3.3.3 Second sound resonances

Already after adding the first doses of ^{3}He into the cell, we observed a feature in the fork response that we had not anticipated on the grounds of earlier work on tuning forks or other oscillators in helium mixture: there appeared sharp peaks in the reso-

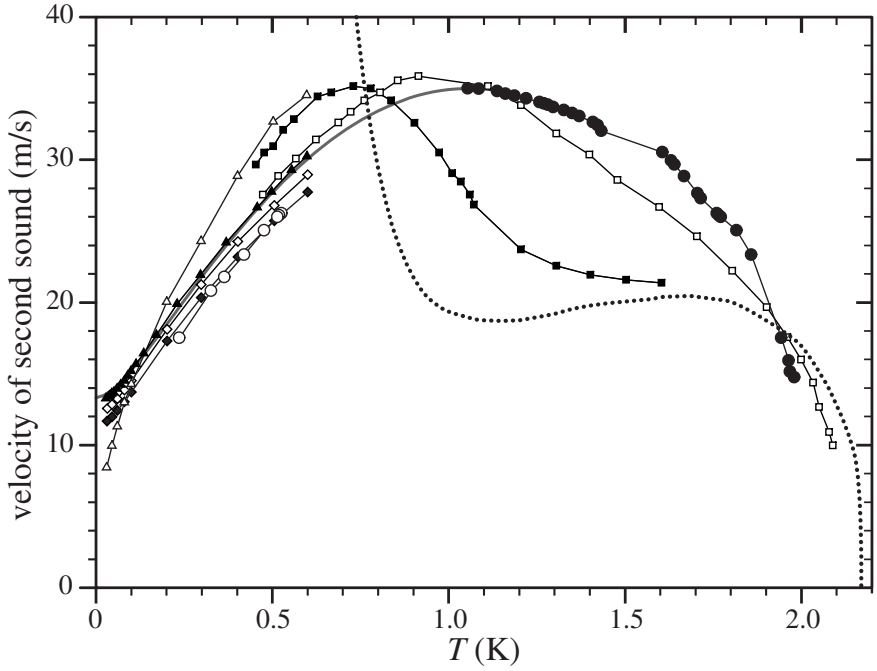

Figure 19: Velocity of second sound in helium liquids: pure ^{4}He at SVP, combined results of various authors (dotted line) [32, 33, 34]; mixtures with ^{3}He concentrations 0.32 % (■) and 4.3 % (□) at SVP after King and Fairbank [35]; 0.153 % (△) and 6.278 % (▲) at SVP, and 5.762 % at 10 atm (◊) and 5.409 % at 20 atm (♦) after Brubaker *et al.* [36]; our approximative results for 8 % at SVP above 1.1 K (●) and for saturated mixture at its melting pressure (○), based on the assumed dependence for 8 % below 1.05 K (gray line).

nance width as a function of temperature, accompanied with variation in the resonance frequency such that in the width–frequency plane, the data formed loops (see Fig. 23). It was obvious that in the system there are a great number of vibrational modes with resonance frequencies rather strongly dependent on the state, particularly temperature, of the mixture. Then, the loop-like behavior in the fork data is observed when the resonance frequency of one of these modes passes the resonance frequency of the fork. It is evident that these vibrational modes originate from the so-called second sound.

Second sound is the notion given to concentration waves propagating in a mixture of a superfluid and a normal fluid, predicted and observed already in early 1940's in ^{4}He as "temperature waves" [28, 29, 30] and little later in dilute helium mixtures, where the oscillation amplitudes of densities of ^{3}He and ^{4}He and temperature are governed by a system of equations given by Brucker *et al.* [31]. Those equations have two solutions, one with the isotopes oscillating in phase—first sound or pressure waves—and the other with opposing oscillation—second sound. At the surface of the fork, the isotopes arguably have the same oscillation amplitude. Because this boundary condition is not necessarily satisfied by pure first sound, the fork is coupled to both first and second sound modes in the mixture. Figure 19 presents a selection of published data on

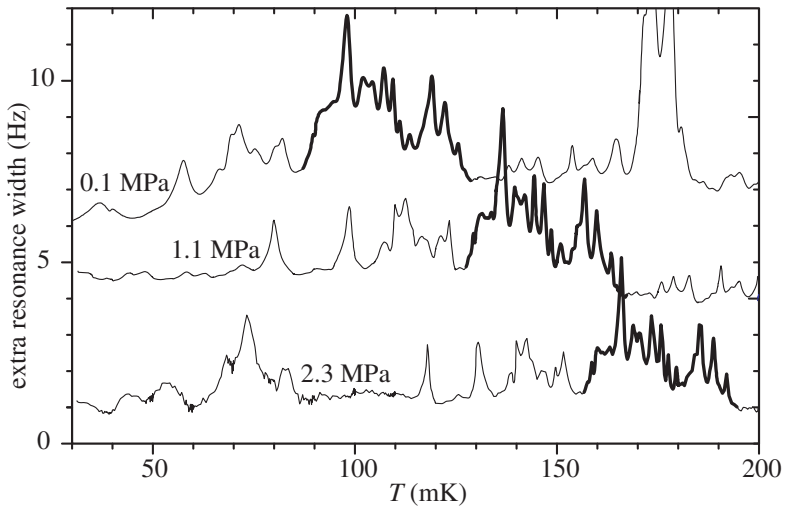

Figure 20: The series of peaks in the resonance width of the tuning fork in saturated mixture at three pressures. Curves have been shifted to improve clarity.

second sound velocity as a function of temperature in ^{4}He and dilute helium mixtures. The plotted data is fully consistent with several features exhibited by our observations. First of all, the magnitude of the velocity of second sound in the conditions of our experiments is such that at frequencies around 32 kHz, the wavelength is of the order of a millimeter, which happens to be the typical length scale of the cross section of the fork and its container. Standing waves of second sound are, therefore, likely to occur inside the fork container. Second, the velocity depends nearly linearly on temperature below 0.5 K covering the same range of values for each concentration and pressure in our experiment, explaining various trends of displacement of the same sequence of resonances in several measurements. See, for example, Fig. 20, which presents the sequence of peaks from 30 to 200 mK in tuning fork data at three pressures. The data were extracted from measurements of the temperature dependence of the resonance width by subtracting a suitable monotonous function of temperature that approximates the contribution of viscous damping at each pressure; at 0.1 MPa, for example, the subtracted function was defined as $\Delta f_2(T) = (700/(T+5) + 0.02T)$ Hz with T in millikelvins. Curves for 0.1 MPa and 1.1 MPa have also been shifted upwards to improve clarity. The ^{3}He content of the sample in each case was close to the low-temperature saturation value. The same pattern is visible in all three graphs, shifting towards higher temperatures because of the similar shift of second sound velocities. Furthermore, the features that start from below 100 mK at 0.1 MPa become narrower at higher temperatures and pressures because the slope of the temperature dependence of the second sound velocity is more shallow in the lower end of the presented temperature range.

The existence of a maximum in the velocity of second sound in helium mixtures, occurring at about 1 K depending on concentration, gives a convincing evidence to the hypothesis that second sound is the cause of the observed resonances. With about 8% of ^{3}He in the mixture sample, we made a slow temperature sweep from the millikelvin regime up to 2 K, and obtained a clear picture that, indeed, is symmetrical about approximately 1.05 K. Figure 21 shows a plot of the data from 0.75 to 1.35 K, with three

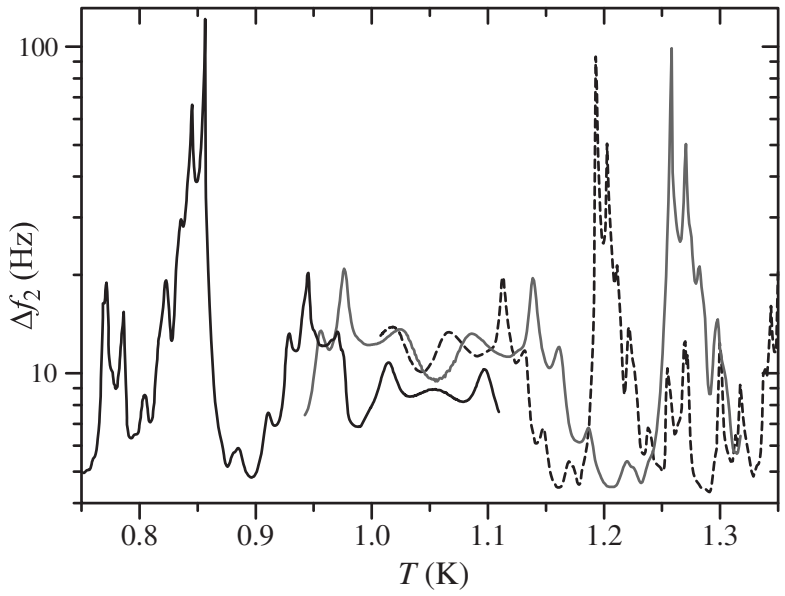

Figure 21: Resonance width of the fork during temperature sweeps around 1 K. The concentration of the mixture was about 8 %, slightly less when measuring the data presented by the solid black curve than for the gray and dashed curves.

curves for slightly different concentrations.

We did not attempt to identify the second sound modes around the tuning fork in any detail—it would require the numerical solution of a wave equation in the complicated three-dimensional geometry of the fork and its container. Besides, the geometry probably varies from fork to fork sufficiently to give each individual fork a unique resonance pattern. Knowing the spectrum of resonant wavelengths would, of course, be useful because then each observed peak could be associated with a certain value of second sound velocity. However, even without this knowledge we can produce some approximative data on the temperature dependence of the second sound velocity, presented by circular symbols in Fig. 19, for saturated mixture at the melting pressure between 0.2 and 0.5 K and for the 8% mixture above 1.05 K. To produce those data, we used the fork data measured in our nominally 8% mixture below 1.05 K as a reference together with an empirical function that estimates the second sound velocity in that case, plotted in Fig. 19 in gray. On the basis of published results and the observed maximum temperature, there is not much freedom in sketching the shape of the temperature dependence in this range. With the empirical function giving the second sound velocity at each peak and other distinguishable feature in the reference data, the same features identified in other measurements can be assumed to mark the same velocity. The two data sets determined by this method are in good agreement with the temperature, pressure, and concentration dependence of earlier results.

Although the second-sound resonances make a disturbing irregularity in the otherwise smooth response of the tuning fork to the viscosity and density of helium mixture, they also offer an interesting prospect for producing a remarkably accurate

reference thermometer. We estimate that the temperature at which a certain second sound resonance occurs can be determined with an accuracy of 10 μK or better in the temperature regime of hundreds of millikelvins where the temperature dependence of second sound velocity is steep. Because of the dependence on pressure and concentration, reproducibility of the resonance temperatures would require constructing a completely closed system or, alternatively, an arrangement with three helium phases, dilute and ^{3}He-rich liquid mixtures and saturated vapor, with the fork immersed in the first-mentioned phase. The latter approach is, obviously, only feasible below the phase-separation temperature of liquid helium mixture, 0.89 K.

3.3.4 Supersaturation and nucleation of pure ^{3}He phase

It is possible to bring a helium mixture to a metastable supersaturated state by changing the pressure or temperature of a homogeneous mixture, initially somewhat below saturation, so that the solubility of ^{3}He falls below the concentration of the sample. Studies of the decay of the supersaturated state by Satoh *et al.* [37] and Tanaka *et al.* [38] suggest that at millikelvin temperatures, it exhibits quantum nucleation, where a virtual nucleus of the pure ^{3}He phase has to tunnel through a potential barrier. Even though the decay of supersaturation must be a stochastic event, the dependence of the decay rate on the excess concentration is such that it is reasonable to speak of a critical supersaturation Δx_{cr}, a typical excess concentration at which the decay occurs. The helium mixture is as close to an ideal system as it can be for studying such a phenomenon in the bulk, because the coating of all surfaces with ^{4}He reduces boundary effects that often play a major role in different nucleation processes in other systems, and there are no impurities whatsoever to act as nucleation centers.

While studying the temperature dependence of the saturation concentration [25], we performed two kinds of operations where supersaturation was produced and, actually, exploited for giving useful reference data: pressure sweeps at constant temperature and temperature sweeps at constant pressure. Pressure sweeps were made in the range between SVP and 0.5 MPa, where the saturation concentration increases quickly as a function of pressure, and their purpose was to find the pressure at which a known amount of ^{3}He at a chosen temperature just dissolves. Temperature sweeps, on the other hand, were performed at higher pressures, and enabled us to directly determine the temperature dependence of solubility. Both kinds of sweep experiments were started with a phase-separated sample with the amount of pure ^{3}He very small in comparison with the mixture phase. Pressure or temperature was first ramped up to induce complete dissolution, and then reduced again. As the solubility decreased below the point of complete dissolution, the mixture entered the supersaturated state, and the developing difference between saturation concentration and the concentration in the homogeneous sample could be detected by comparing tuning fork data recorded in the two cases. Eventually, the pure ^{3}He phase reappeared in the cell, which was detected by the fork as a rapid relaxation of the mixture phase into the saturation concentration. As examples of both kinds of operations, Fig. 22 shows fork data in a pressure sweep experiment at 10 mK below 0.1 MPa, and Fig. 23 in a temperature sweep experiment at 2.4 MPa. Although the loops (caused by second sound resonances, see above) complicate the picture in the temperature sweep somewhat, the data indicate clearly the course of the process.

In both kinds of sweep experiments, the change of the fork response indicating the relaxation from supersaturation to the saturated mixture can be converted into the amount of excess concentration at the moment of the nucleation of the pure ^{3}He phase.

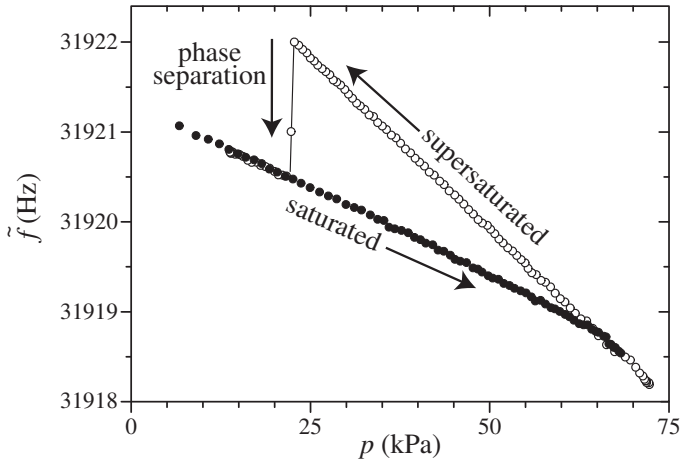

Figure 22: Fork data recorded during a pressure sweep experiment at 10 mK. Arrows indicate the direction of time.

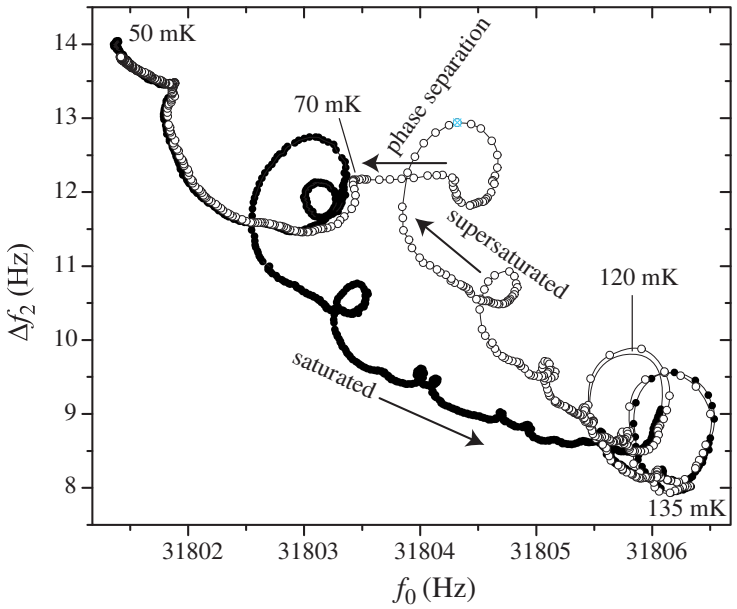

Figure 23: Fork data and some temperature readings recorded during a temperature sweep experiment at 2.4 MPa: warming (•) and cooling (○). Arrows indicate the direction of time.

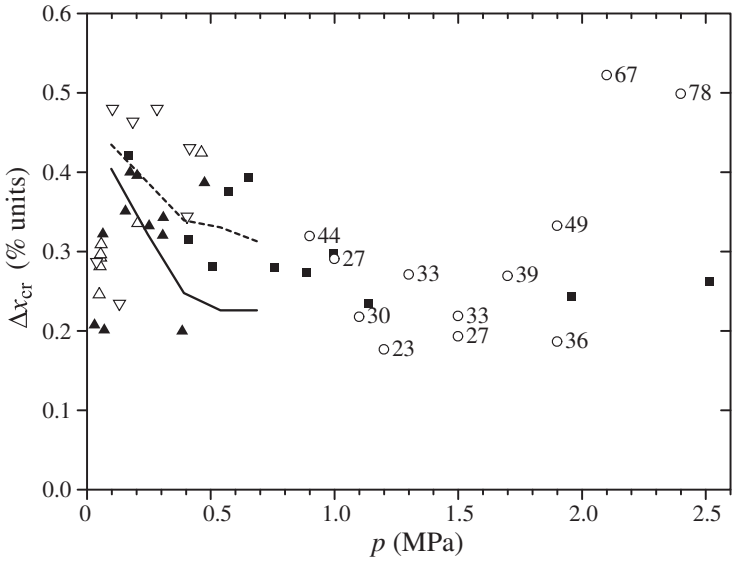

Figure 24: Critical supersaturation of helium mixture. Excess concentrations reached by our temperature sweeps at constant pressure (○ and temperature at phase separation in millikelvins), pressure sweeps at 10 mK (■), and pressure sweeps at temperatures between 5–12 mK (▲), 22–43 mK (△), and 50–80 mK (▽). Critical supersaturation according to Tanaka *et al.*[38] at 10 mK (solid line) and at 50 mK (dashed line).

The data accumulated over our measurements are presented in Fig. 24 together with Δx_{cr} curves adopted from Tanaka *et al.* who made measurements up to 0.8 MPa only. Our data are rather fragmentary because the statistics of the nucleation process was not the main subject of our work, but still allow comparison with Tanaka's results. They appear to agree well, both in overall magnitude and, at least qualitatively, in the pressure and temperature dependencies. Moreover, our data do not significantly depend on whether supersaturation was reached by varying temperature or pressure, which can be considered as further evidence that the critical supersaturation indeed is a property intrinsic to the bulk mixture. Below 0.1 MPa, the excess concentrations reached by us are only about half of the general level, which is probably related to the fact that below the atmospheric pressure, the liquid–vapor interfaces in the filling lines lying somewhere between the cell and the 4 K bath made it difficult to change the pressure smoothly.

3.3.5 Results in pure ^{3}He

We studied the fork response in pure normal ^{3}He liquid at five pressures: 0.1, 0.5, 1.0, 1.7, and 2.56 MPa, the highest value set by the melting pressure of the saturated mixture also present in the cell. Figure 25 shows the measured resonance widths as a function of temperature, and calculated curves for the lowest and highest pressures, based on the vibrating wire theory. Viscosity and density of ^{3}He were taken from literature and an equivalent wire radius of 0.15 mm was applied. Agreement with the 0.1 MPa data is good, whereas at the melting pressure, theory predicts a notably higher damping than that observed. The slope of the temperature dependence is very well reproduced by

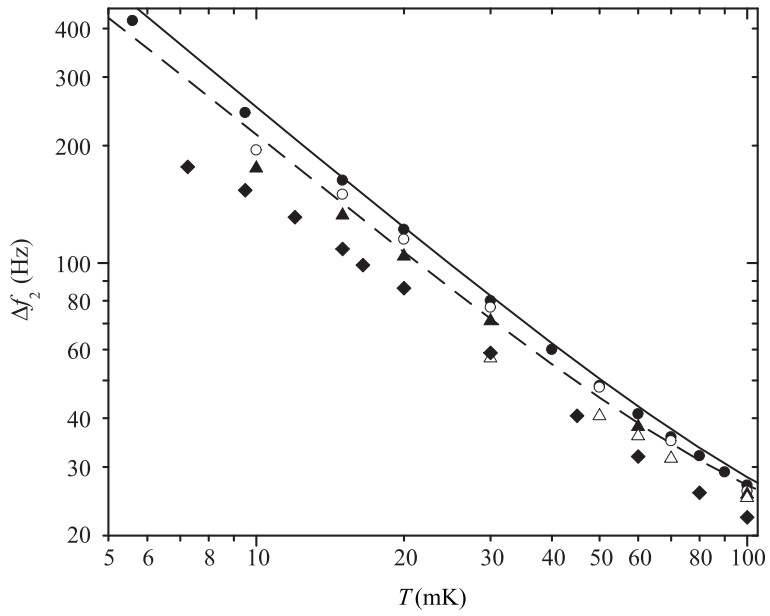

Figure 25: Resonance width of the quartz fork in normal pure ^{3}He at five pressures: 0.1 MPa (●), 0.5 MPa (○), 1.0 MPa (▲), 1.7 MPa (△), and 2.56 MPa (⧫). Calculated curves for a cylindrical wire with radius of 0.15 mm in ^{3}He at 0.1 MPa (solid line) and at 2.56 MPa (dashed line).

theory at both pressures, suggesting that whatever the cause of the slope discrepancy is in the case of mixtures, it is not present in pure ^{3}He.

The fork data in pure ^{3}He at the applied pressures are shown in Fig. 26 on the resonance width–frequency plane. At each pressure, the data points trace a smooth arc, free of loops and bends visible in mixture data. This supports the picture that the resonances in mixtures originate from second sound, as in normal pure ^{3}He there is no such mode.

4 Conclusions

In our experiment on refrigerating helium mixtures by demagnetization of copper, vibrating wire response was measured across more than four orders of magnitude in temperature, from the conventional hydrodynamic regime of the diluted ^{3}He to the far developed ballistic limit. On the basis of measurements in the hydrodynamic regime, we obtained data on the viscosity of dilute mixtures as a function of concentration that supplement and agree with previous studies. Results beyond the regime of hydrodynamic description suggest that the scattering of ^{3}He quasiparticles from the wire is partially specular, more so at higher concentrations than lower. To obtain a more qualitative understanding of the degree of specularity, a theory is needed that takes into account both specular and diffuse scattering. In addition to specularity whose effect was notable over a wide range of temperatures, in the ballistic regime effects from the finiteness of the experimental volume were also observed, in confirmation to theoretical

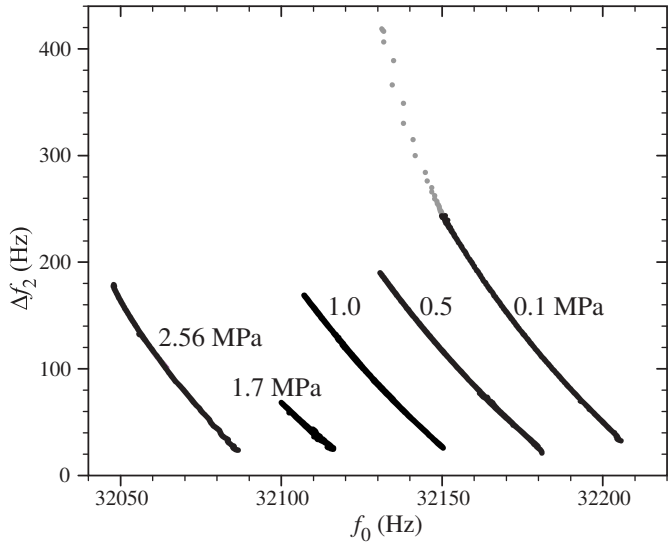

Figure 26: Fork response in normal pure ^{3}He at five pressures, shown in MPa, in the frequency–width plane. For the corresponding temperatures, see the previous figure. Data shown in gray (0.1 MPa, lowest temperature) were obtained by measuring full resonance spectra, and black points by the single-frequency method.

work on the subject.

In contrast to vibrating wires, there is no analytically justified expression of damping experienced by a tuning fork as a function of properties of the surrounding liquid. The existing theory for cylindrical wires can be adjusted to reproduce fork data in pure normal ^{3}He by applying a fitted equivalent value of the wire radius, whereas in dilute helium mixtures, the observed temperature dependence is less steep than the wire theory predicts regardless of the equivalent radius. Because this deviation is specific to forks in mixtures, the reason may be related to a phenomenon that strikingly manifested itself in fork experiments in mixtures, viz. second sound. On the basis of the observed resonances, it is evident that the fork emits second sound, and this emission necessarily adds to the damping.

Due to the lack of an analytical description of viscous damping in their geometry, forks cannot serve as primary viscometers, but once calibrated, they are very useful sensors of the state of helium liquids. Good signal quality enables fast and accurate single-point measurement, and owing to their lower density, larger size, and higher frequency in comparison with typical vibrating wires, the resonance quality factor remains higher and sensitivity to changes in liquid density is better.

Acknowledgements

We appreciate the contributions of Juha Martikainen to the first of the three experiments described, particularly for constructing the experimental cell. This work was supported by the Academy of Finland through Grant No. 213496, the Finnish Programme for Centres of Excellence in Research in 2002–2007 and 2006–2011, and the funding decisions No. 202235 and No. 112994. We also acknowledge the EC-funded

ULTI Project (Transnational Access in Programme FP6, Contract No. RITA-CT-2003-505313) and the grants from Finnish National Graduate School in Materials Physics and the Viljo, Yrjö and Kalle Väisälä Foundation.

References

[1] G. G. Stokes, *Mathematical and Physical Papers*, vol. 3 (Cambridge University Press, London, 1901).

[2] R. König and F. Pobell, J. Low Temp. Phys. **97**, 287 (1994).

[3] H. Højgaard Jensen, H. Smith, P. Wölfle, K. Nagai, and T. Maack Bisgaard, J. Low Temp. Phys. **41**, 473 (1980).

[4] D. C. Carless, H. E. Hall, and J. R. Hook, J. Low Temp. Phys. **50**, 583 (1983).

[5] R. M. Bowley and J. R. Owers-Bradley, J. Low Temp. Phys. **136**, 15 (2004).

[6] D. Einzel, P. Panzer, and M. Liu, Phys. Rev. Lett. **64**, 2269 (1990).

[7] A. M. Guénault, V. Keith, C. J. Kennedy, and G. R. Pickett, Phys. Rev. Lett. **50**, 522 (1983).

[8] D. C. Carless, H. E. Hall, and J. R. Hook, J. Low Temp. Phys. **50**, 605 (1983).

[9] S. Perisanu and G. Vermeulen, Phys. Rev. B **73**, 134517 (2006).

[10] T. H. Virtanen and E. V. Thuneberg, in *Low Temperature Physics: 24th International Conference on Low Temperature Physics – LT24* (AIP, New York, 2006), vol. 850 of *AIP Conf. Proc.*, pp. 113–114.

[11] T. H. Virtanen and E. V. Thuneberg (2008), submitted to the proceedings of 25th International Conference on Low Temperature Physics – LT25.

[12] T. H. Virtanen and E. V. Thuneberg, private communication.

[13] A. M. Guénault, V. Keith, C. J. Kennedy, S. G. Mussett, and G. R. Pickett, J. Low Temp. Phys. **62**, 511 (1986).

[14] J. Martikainen and J. T. Tuoriniemi, J. Low Temp. Phys. **124**, 367 (2001).

[15] E. Pentti, Master's thesis, Helsinki University of Technology (2003).

[16] E. Tanaka, K. Hatakeyama, S. Noma, and T. Satoh, Cryogenics **40**, 365 (2000).

[17] G. E. Watson, J. D. Reppy, and R. C. Richardson, Phys. Rev. **188**, 384 (1969).

[18] E. Krotscheck, M. Saarela, K. Schörkhuber, and R. Zillich, Phys. Rev. Lett. **80**, 4709 (1998).

[19] J. Martikainen, J. Tuoriniemi, T. Knuuttila, and G. Pickett, J. Low Temp. Phys. **126**, 139 (2002).

[20] J. Martikainen, J. Tuoriniemi, E. Pentti, and G. Pickett, Physica B **329-333**, 178 (2003).

[21] R. König, Ph.D. thesis, Universität Bayreuth (1993).

[22] A. P. Sebedash, J. T. Tuoriniemi, S. T. Boldarev, E. M. M. Pentti, and A. J. Salmela, J. Low Temp. Phys. **148**, 725 (2007).

[23] J. Bardeen, G. Baym, and D. Pines, Phys. Rev. **156**, 207 (1967).

[24] I. A. Todoshchenko, H. Alles, A. Babkin, A. Ya. Parshin, and V. Tsepelin, J. Low Temp. Phys. **126**, 1449 (2002).

[25] E. M. Pentti, J. T. Tuoriniemi, A. J. Salmela, and A. P. Sebedash, Phys. Rev. B **78**, 064509 (2008).

[26] D. O. Clubb, O. V. L. Buu, R. M. Bowley, R. Nyman, and J. R. Owers-Bradley, J. Low Temp. Phys. **136**, 1 (2004).

[27] R. Blaauwgeers, M. Blazkova, M. Človečko, V. B. Eltsov, R. de Graaf, J. Hosio, M. Krusius, D. Schmoranzer, W. Schoepe, L. Skrbek, et al., J. Low Temp. Phys. **146**, 537 (2007).

[28] L. Landau, J. Phys. USSR **5**, 71 (1941).

[29] L. Tisza, Phys. Rev. **72**, 838 (1947).

[30] V. Peshkov, J. Phys. USSR **10**, 389 (1946).

[31] H. Brucker, Y. Disatnik, and R. Meyuhas, J. Low Temp. Phys. **24**, 193 (1976).

[32] C. T. Lane, H. A. Fairbank, and W. M. Fairbank, Phys. Rev. **71**, 600 (1947).

[33] R. D. Maurer and M. A. Herlin, Phys. Rev. **76**, 948 (1949).

[34] D. de Klerk, R. P. Hudson, and J. R. Pellam, Phys. Rev. **93**, 28 (1954).

[35] J. C. King and H. A. Fairbank, Phys. Rev. **93**, 21 (1954).

[36] N. R. Brubaker, D. O. Edwards, R. E. Sarwinski, P. Seligmann, and R. A. Sherlock, J. Low Temp. Phys. **3**, 619 (1970).

[37] T. Satoh, M. Morishita, M. Ogata, and S. Katoh, Phys. Rev. Lett. **69**, 335 (1992).

[38] E. Tanaka, K. Hatakeyama, S. Noma, S. N. Burmistrov, and T. Satoh, J. Low Temp. Phys. **127**, 81 (2002).